Analysis of the electrically forced vibrations of piezoelectric mesa resonators*

He Hui-Jing(何慧晶)[a)b)], Nie Guo-Quan(聂国权)[a)], Liu Jin-Xi(刘金喜)[a)], and Yang Jia-Shi(杨嘉实)[b)†]

[a)] *Department of Engineering Mechanics, Shijiazhuang Tiedao University, Shijiazhuang* 050043, *China*
[b)] *Department of Mechanical and Materials Engineering, University of Nebraska-Lincoln, Lincoln, NE* 68588-0526, *USA*

(Received 13 January 2013; revised manuscript received 25 January 2013)

We study the electrically forced thickness-shear and thickness-twist vibrations of stepped thickness piezoelectric plate mesa resonators made of polarized ceramics or 6-mm class crystals. A theoretical analysis based on the theory of piezoelectricity is performed, and an analytical solution is obtained using the trigonometric series. The electrical admittance, resonant frequencies, and mode shapes are calculated, and strong energy trapping of the modes is observed. Their dependence on the geometric parameters of the resonator is also examined.

Keywords: crystal, plate, resonance, resonator

PACS: 77.65.Fs, 77.65.–j **DOI:** 10.1088/1674-1056/22/8/087704

1. Introduction

Piezoelectric crystals are widely used to make resonators, filters, sensors, and other acoustic wave devices for time-keeping, frequency generation and operation, telecommunication, and sensing. Thickness-shear (TSh) vibrations of crystal plates are common structures and modes for these applications.[1,2] TSh modes can be excited in quartz plates, ceramic plates with in-plane poling, plates of 6-mm class crystals with in-plane six-fold axes, etc. Theoretically, pure TSh modes can only exist in unbounded plates without edge effects. When a plate is vibrating in TSh mode, the motions of the material particles are parallel to the surfaces of the plate, and the particle velocities vary only along the plate thickness, without in-plane variations. In reality, however, due to the finite sizes of devices, pure TSh modes cannot exist because of edge effects. In real devices, the actual TSh operating modes have slow, in-plane variations. These modes are referred to as transversely varying TSh modes.[3] In cases where the in-plane mode variation is along the direction perpendicular to the TSh particle velocity, the modes are called thickness-twist (TT) modes.[4,5]

When a plate vibrates in the TSh modes, all parts of the plate are moving, except for some of the planes parallel to the plate surface (nodal planes). For such a vibrating plate, the mounting that is necessary for any device, becomes an issue. Fortunately, the TSh modes in a plate with partial electrodes in the center (trapped energy resonator) have an important and useful behavior called energy trapping, through which the TSh vibration is confined under the electrodes and decays rapidly outside them.[6] Energy trapping is useful in device mounting. For trapped modes, mounting can be done near the plate edges without affecting the vibration of the plate. Energy trapping is mainly due to the inertial effect of the electrodes.[6] Piezoelectric coupling can also contribute to energy trapping,[7] and researchers have developed contoured resonators[8–11] from plates with gradually varying thicknesses and mesa resonators[12–21] from plates with stepped or piecewise constant thickness. In contoured or mesa resonators, the changing plate thickness usually leads to stronger energy trapping than the inertia of the partial electrodes.

This paper is mainly concerned with mesa resonators. Because of the change in plate thickness, analytical modeling of mesa resonators is mathematically challenging. Theoretical results are few and scattered. The analysis in Ref. [12] was based on approximate, two-dimensional plate equations. In Refs. [13]–[20], a combined analytical–numerical approach, a finite-element numerical method, and an experimental study were conducted. Most of Refs. [12]–[21] presented the results on mode variation along the direction of the particle velocity. Only references [18] and [21] have results on mode variation along the direction perpendicular to the particle velocity. These results are for free vibration frequency and mode shape analysis only.

In real applications, resonators operate as elements of electrical circuits. Two of the basic properties of a resonator, its resonant frequency and its electrical admittance, are of primary interest for a complete circuit analysis. The impedance of a resonator can only be obtained from an electrically forced vibration analysis. A review of the relevant literature shows that two aspects of mesa resonators are rarely studied. One is the electrically forced vibration and the other the in-plane mode variation perpendicular to particle velocity. In this paper,

*Project supported by the National Natural Science Foundation of China (Grant No. 11272222) and the National Key Basic Research Program of China (Grant No. 2012CB723300).

†Corresponding author. E-mail: jyang1@unl.edu

© 2013 Chinese Physical Society and IOP Publishing Ltd

for a complete simulation of an operating mesa resonator, we perform an electrically forced vibration analysis of a mesa resonator for its electrical admittance, and examine the effects of the geometric parameters of the resonator on its basic behaviors including admittance, resonant frequencies, mode shapes, and energy trapping. In-plane mode variation perpendicular to particle velocity is considered. Our analysis differs from all previous analyses of mesa resonators in the literature in that the present analysis is based on the exact equations of linear piezoelectricity.

2. Governing equations

Consider the plate made of polarized ceramics or crystals of 6-mm class as shown in Fig. 1. The mathematical structures of the material tensors of polarized ceramics and 6-mm class crystals are the same. The analysis below is valid for both materials. Polarized ceramics are conventional materials for resonant piezoelectric devices, and 6-mm class crystals include aluminum nitride and zinc oxide, which are of current and growing research interest for thin-film acoustic wave resonators and sensors.[22–26] The plate is unbounded in the x_3 direction and does not vary along x_3. Figure 1 shows a cross section of the plate. The poling direction or the six-fold axis is along x_3. The entire surface of the plate is traction free. Across the electrodes, shown by the thick lines at the top and bottom of the central portion of the plate, a voltage of $2V\exp(\mathrm{i}\omega t)$ is applied. We consider a plate driven by an electric field in the plate thickness direction or the so-called thickness field excitation (TFE). A plate can also be driven by an in-plane electric field or the so-called lateral field excitation (LFE).[27–29] Due to the symmetry in the structure and the antisymmetry of the applied voltage about the plate middle plane, the plate is driven into shear-horizontal (SH) or antiplane[30] motions, even in x_1 and odd in x_2. We artificially divide the plate cross section by dotted lines into three rectangular regions, and call them the top, middle, and bottom regions.

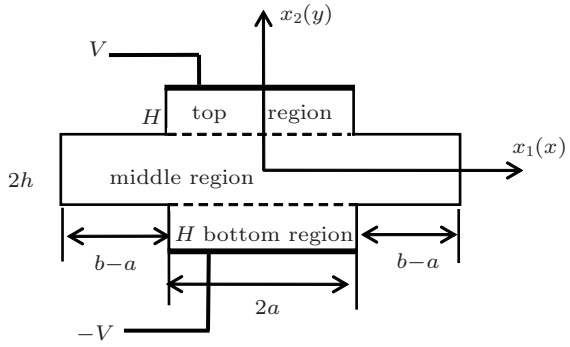


Fig. 1. A mesa resonator of polarized ceramics or 6-mm class crystals.

The direction x_3 is determined from directions x_1 and x_2 by the right-hand rule.

For the mesa resonator in Fig. 1, SH motions including the TSh and TT modes are governed by[30,31]

$$u_1 = u_2 = 0,$$
$$u_3 = u(x_1,x_2,t), \quad \phi = \phi(x_1,x_2,t), \tag{1}$$

where u_1, u_2, and u_3 are the components of the displacement vector, and ϕ is the electric potential. A function ψ can be introduced through $\phi = \psi + eu/\varepsilon$,[30,31] where $e = e_{15}$ and $\varepsilon = \varepsilon_{11}$ are the relevant piezoelectric and dielectric constants. The governing equations for u and ψ are[30,31]

$$\bar{c}\nabla^2 u = \rho\ddot{u}, \quad \nabla^2\psi = 0, \tag{2}$$

where ∇^2 is the two-dimensional Laplacian, $\bar{c} = c + e^2/\varepsilon$, and $c = c_{44}$ is the relevant shear elastic constant. The nonzero stress components are $T_{23} = T_4$ and $T_{13} = T_5$. The nonzero electric displacement components are D_1 and D_2. They are given by the following constitutive relations:[30,31]

$$T_{23} = \bar{c}u_{,2} + e\psi_{,2}, \quad T_{13} = \bar{c}u_{,1} + e\psi_{,1},$$
$$D_1 = -\varepsilon\psi_{,1}, \quad D_2 = -\varepsilon\psi_{,2}, \tag{3}$$

where an index after the comma denotes partial differentiation with respect to the coordinate associated with the index. The above equations are valid in each rectangular region in Fig. 1. The boundary conditions at the top of the central potion are

$$T_{23}(x_1,h+H,t) = 0, \quad |x_1| < a,$$
$$\varphi(x_1,h+H,t) = V\exp(\mathrm{i}\omega t), \quad |x_1| < a. \tag{4}$$

The boundary and continuity conditions at the interface between the top and middle rectangular regions are

$$u(x_1,h^-,t) = u(x_1,h^+,t), \quad |x_1| < a, \tag{5a}$$
$$\varphi(x_1,h^-,t) = \varphi(x_1,h^+,t), \quad |x_1| < a, \tag{5b}$$
$$T_{23}(x_1,h^-,t) = \begin{cases} T_{23}(x_1,h^+,t), & |x_1| < a, \\ 0, & a < |x_1| < b, \end{cases} \tag{5c}$$
$$D_2(x_1,h^-,t) = \begin{cases} D_2(x_1,h^+,t), & |x_1| < a, \\ 0, & a < |x_1| < b. \end{cases} \tag{5d}$$

The right edges of the top and middle rectangular regions are traction free, with

$$T_{13}(a,x_2,t) = 0, \quad h < |x_2| < h+H,$$
$$D_1(a,x_2,t) = 0, \quad h < |x_2| < h+H, \tag{6}$$

$$T_{13}(b,x_2,t) = 0, \quad |x_2| < h,$$
$$D_1(b,x_2,t) = 0, \quad |x_2| < h. \tag{7}$$

Due to antisymmetry and symmetry, the boundary and continuity conditions at the lower interface, the bottom surface, and the left edges are not needed. In formulating the above boundary conditions, the electrodes are assumed to be very thin so their mechanical effects are neglected. The free charge on and

the current that flows into the electrode at $x_2 = H + h$ are given by[32]

$$q = \int_{-a}^{a} -D_2|_{x_2=h+H}\,\mathrm{d}x_1, \quad I = \dot{q}, \tag{8}$$

where a unit dimension in the x_3 direction is taken. In time-harmonic motions, the admittance Y of the device is given by

$$Y = \frac{I}{2V}. \tag{9}$$

3. Series solution

For time-harmonic motions, we use the usual complex notation and write u, ψ, ϕ, T_{23}, D_2, q, and I as

$$\begin{aligned}&(u,\psi,\varphi,T_{23},D_2,q,I)\\ &= \mathrm{Re}\{(U,\Psi,\Phi,T,D,Q,\bar{I})\exp(\mathrm{i}\omega t)\}.\end{aligned} \tag{10}$$

We will write solutions in the top and middle rectangular regions using the trigonometric series with undetermined coefficients. The fields in the bottom rectangular region are not needed due to symmetry. Then, the solutions in different regions will be substituted into the interface continuity conditions among different regions to obtain linear algebraic equations for the undetermined coefficients.

3.1. Middle-region fields

In this region, we construct the following solution from the standard method of separation of variables in partial differential equations:

$$U = B_0\sin(\eta_0 y) + \sum_{m=1}^{\infty} B_m \sin(\eta_m y)\cos\frac{m\pi x}{b}, \tag{11}$$

$$\Psi = D_0 y + \sum_{m=1}^{\infty} D_m \sinh\frac{m\pi y}{b}\cos\frac{m\pi x}{b}, \tag{12}$$

where B_m and D_m are undetermined constants, (x, y) correspond to (x_1, x_2), and

$$\eta_m^2 = \frac{\rho\,\omega^2}{\bar{c}} - \left(\frac{m\pi}{b}\right)^2, \quad m = 0,1,2,3,\ldots. \tag{13}$$

Equations (11) and (12) satisfy Eqs. (2) and (7). To apply the boundary and continuity conditions at $x_2 = h$, from Eqs. (11) and (12), we obtain the following expressions:

$$\begin{aligned}\Phi &= \frac{e}{\varepsilon}B_0\sin(\eta_0 y) + D_0 y + \sum_{m=1}^{\infty}\left[\frac{e}{\varepsilon}B_m\sin(\eta_m y)\right.\\ &\quad \left. + D_m\sinh\frac{m\pi y}{b}\right]\cos\frac{m\pi x}{b},\end{aligned} \tag{14}$$

$$\begin{aligned}T &= \bar{c}B_0\eta_0\cos(\eta_0 y) + eD_0 + \sum_{m=1}^{\infty}\left[\bar{c}B_m\eta_m\cos(\eta_m y)\right.\\ &\quad \left. + eD_m\frac{m\pi}{b}\cosh\frac{m\pi y}{b}\right]\cos\frac{m\pi x}{b},\end{aligned} \tag{15}$$

$$D = -\varepsilon D_0 + \sum_{m=1}^{\infty} -\varepsilon\frac{m\pi}{b}D_m\cosh\frac{m\pi y}{b}\cos\frac{m\pi x}{b}. \tag{16}$$

3.2. Top-region fields

Similarly, in this region, the general solution symmetric in x can be written as

$$\begin{aligned}U &= F_0\sin(\xi_0 y) + G_0\cos(\xi_0 y) + \sum_{m=1}^{\infty}[F_m\sin(\xi_m y)\\ &\quad + G_m\cos(\xi_m y)]\cos\frac{m\pi x}{a},\end{aligned} \tag{17}$$

$$\begin{aligned}\Psi &= H_0 y + K_0 + \sum_{m=1}^{\infty}\left[H_m\sinh\frac{m\pi y}{a}\right.\\ &\quad \left. + K_m\cosh\frac{m\pi y}{a}\right]\cos\frac{m\pi x}{a},\end{aligned} \tag{18}$$

where F_m, G_m, H_m, and K_m are undetermined constants, and

$$\xi_m^2 = \frac{\rho\,\omega^2}{\bar{c}} - \left(\frac{m\pi}{a}\right)^2, \quad m = 0,1,2,3,\ldots. \tag{19}$$

Equations (17) and (18) satisfy Eqs. (2) and (6). To apply the boundary and continuity conditions at $x_2 = h$ and $x_2 = h + H$, we need

$$\begin{aligned}\Phi &= H_0 y + K_0 + \frac{e}{\varepsilon}F_0\sin(\xi_0 y) + \frac{e}{\varepsilon}G_0\cos(\xi_0 y)\\ &\quad + \sum_{m=1}^{\infty}\left[\frac{e}{\varepsilon}F_m\sin(\xi_m y) + \frac{e}{\varepsilon}G_m\cos(\xi_m y)\right.\\ &\quad \left. + H_m\sinh\frac{m\pi y}{a} + K_m\cosh\frac{m\pi y}{a}\right]\cos\frac{m\pi x}{a},\end{aligned} \tag{20}$$

$$\begin{aligned}T &= \bar{c}\xi_0 F_0\cos(\xi_0 y) - \bar{c}\xi_0 G_0\sin(\xi_0 y) + eH_0\\ &\quad + \sum_{m=1}^{\infty}\left[\bar{c}\xi_m F_m\cos(\xi_m y) - \bar{c}\xi_m G_m\sin(\xi_m y)\right.\\ &\quad + e\frac{m\pi}{a}H_m\cosh\frac{m\pi y}{a}\\ &\quad \left. + e\frac{m\pi}{a}K_m\sinh\frac{m\pi y}{a}\right]\cos\frac{m\pi x}{a},\end{aligned} \tag{21}$$

$$\begin{aligned}D &= -\varepsilon H_0 + \sum_{m=1}^{\infty}\left[-\varepsilon\frac{m\pi}{a}H_m\cosh\frac{m\pi y}{a}\right.\\ &\quad \left. - \varepsilon\frac{m\pi}{a}K_m\sinh\frac{m\pi y}{a}\right]\cos\frac{m\pi x}{a}.\end{aligned} \tag{22}$$

3.3. Boundary and continuity conditions

The substitution of Eqs. (11), (12), (14)–(16), (17), (18), and (20)–(22) into Eqs. (4) and (5) yields six equations in terms of trigonometric series. We then multiply both sides of the four equations from Eqs. (4), 5(a), and 5(b) by $\cos(n\pi x/a)$ $(n = 0,1,2,\ldots)$ and integrate the resulting equations over $(-a, a)$, then multiply both sides of the two equations from Eqs. 5(c) and 5(d) by $\cos(n\pi x/b)$ $(n = 0,1,2,\ldots)$ and integrate the resulting equations over $(-b, b)$. This leads to a system of linear algebraic equations for the undetermined constants B_m, D_m, F_m, G_m, H_m, and K_m. These equations are solved using a computer.

4. Numerical results

As a numerical example, we consider a mesa resonator made of polarized ceramics, PZT-4.[33] Damping is introduced using a complex elastic constant. We let $c_{44} = c_{44}(1 + \mathrm{i}/Q)$, where Q is a large and positive real number (the mechanical quality factor). $Q = 20$, $V = 110$ V, $2a = 15$ mm, $2b = 40$ mm, $2h = 1$ mm, and $H = 0.3$ mm are used. The admittance is determined by the resonator structure and is independent of the applied voltage used to calculate it. We also introduce a reference circular frequency

$$\omega_0 = \frac{\pi}{2(h+H)}\sqrt{\frac{c_{44}}{\rho}} = 3.627599 \times 10^6 \text{ rad}\cdot\text{s}^{-1}, \quad (23)$$

which is the fundamental TSh frequency of a ceramic plate with a thickness of $(h+H)$.

Figure 2(a) shows the admittance versus the driving frequency. Two resonance peaks are visible near $\omega/\omega_0 = 1$, with one much larger than the other. The numerical data show that in fact there is also a third peak, which is small and cannot be seen in the figure. Figures 2(b)–2(d) show the real and imaginary parts of the displacement component u_3 at these three resonances, respectively. The imaginary part of the first mode is much larger than the rest and is the main contributor to the larger peak in Fig. 2(a). These modes are all trapped in the thick central portion of the plate (energy trapping). Within the central portion of the plate, the three modes all pass through zero only once along the plate thickness direction. The first mode has no zeros, i.e., no nodal points between $(-a, a)$ along the x direction. It is a slowly varying TSh mode. The second and the third modes have two and four nodal points along x, respectively, and are TT modes. The frequencies of these modes are mainly determined by $2(H+h)$, i.e., the thickness of the central portion of the plate. They are slightly above ω_0 and are slowly increasing as the wavelength along x becomes shorter. The presence of nodal points along x causes charge cancellation on the electrodes and is responsible for the drastic drop of admittance from the first mode to the second mode and the third mode. The u_3 of the first mode is slowly varying along x. The trigonometric series converges rapidly. When eight terms are used for the relatively long region in the middle and three terms are used for the relatively short region at the top, the frequency has three significant figures. For the second mode and the third mode with more variations along x, more terms in the series are needed for the same accuracy. Numerical data show that at higher frequencies there are other resonances whose admittances are even smaller.

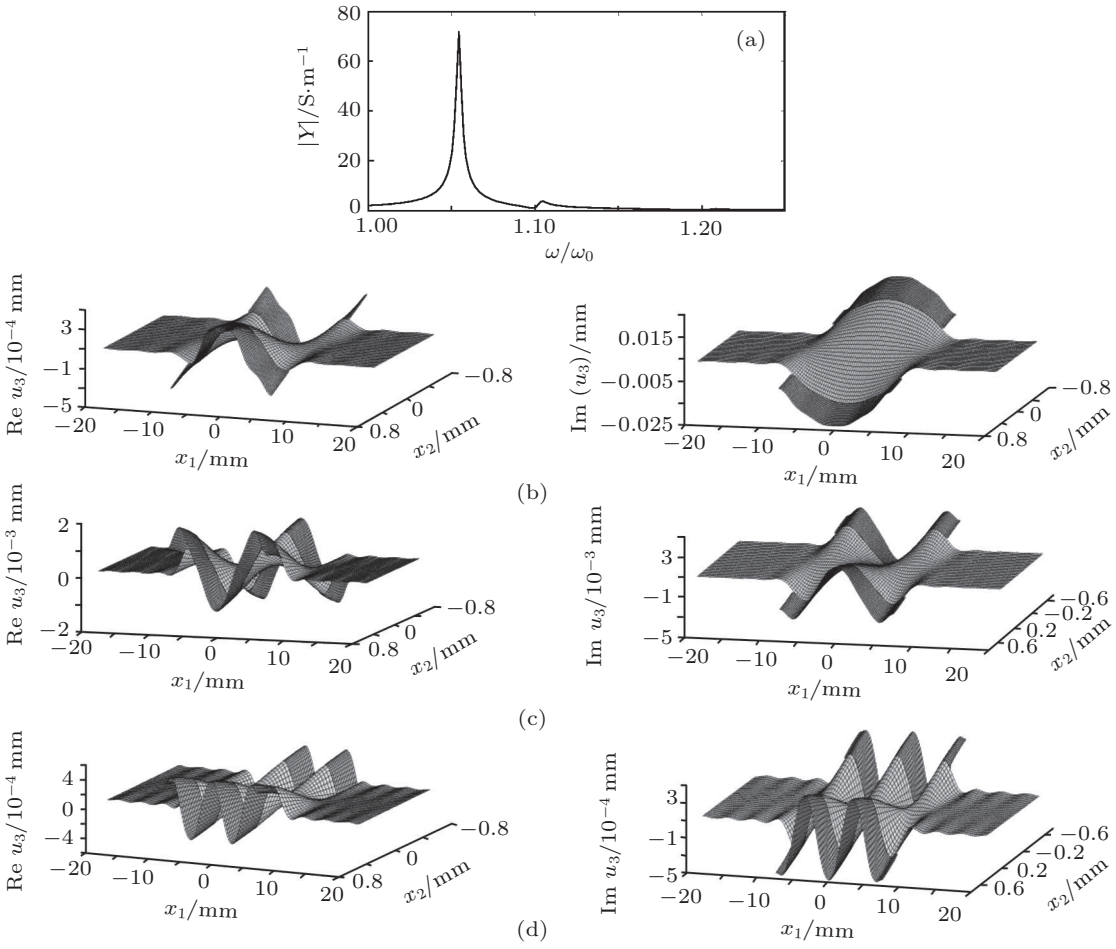


Fig. 2. (a) Admittances versus driving frequency. (b) The first mode with $\omega_1 = 3.826517 \times 10^6$ rad·s^{-1}. (c) The second mode with $\omega_2 = 4.012095 \times 10^6$ rad·s^{-1}. (d) The third mode with $\omega_3 = 4.400648 \times 10^6$ rad·s^{-1}.

Figure 3(a) shows the effect of $2a$, i.e., the length of the thick central portion of the resonator, on the admittance. When a becomes larger, the electrodes become longer and can collect more charges. Therefore, the admittance becomes larger as expected. a also affects the resonance frequencies. As a increases, the thick portion of the plate becomes longer and has more inertia and hence lower resonant frequency. Figures 3(b) and 3(c) show the effects of a on the first two modes. For larger values of a, the modes spread more toward the edges or are less trapped. Corresponding to $a = 7.5$, 9.5, and 11.5 mm, the resonant frequencies of the first mode are 3.826517×10^6 rad$\cdot$s^{-1}, 3.819001×10^6 rad$\cdot$s^{-1}, and 3.814545×10^6 rad$\cdot$s^{-1}, respectively. As expected, the frequencies become lower as a increases.

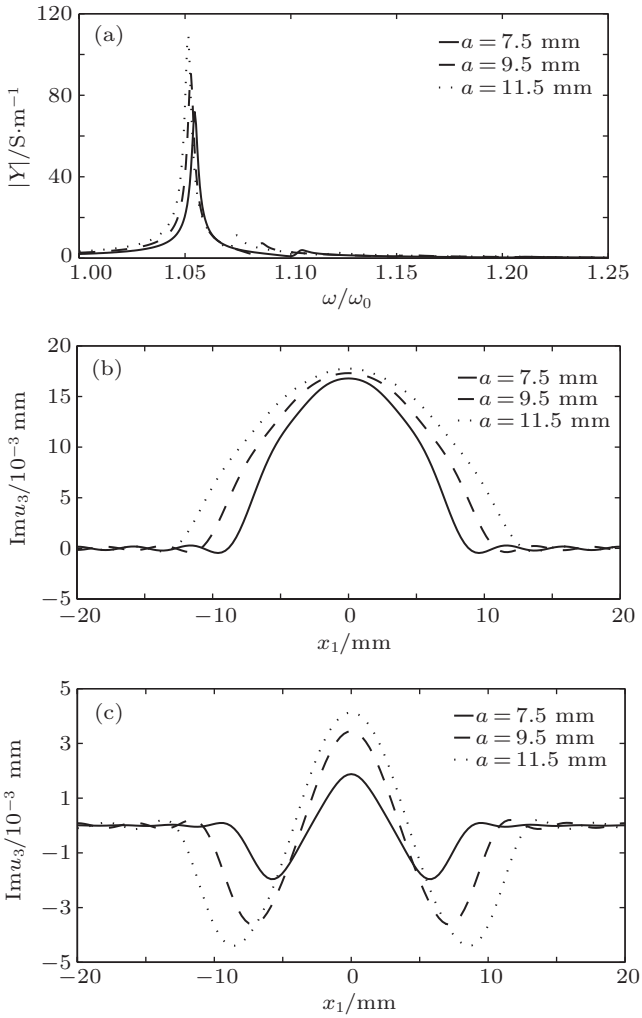


Fig. 3. The effects of a when $H = 0.3$ mm. (a) Admittance, (b) Im$\{u_3(h)\}$ of the first mode, and (c) Im$\{u_3(h)\}$ of the second mode.

Figure 4(a) shows the effect of $2H$, i.e., the difference between the thickness of the central portion and the edge, on the admittance of the resonator. When H becomes larger, the admittance becomes smaller. This is because the plate vibration amplitude becomes smaller, as seen from Figs. 4(b) and 4(c). From Figs. 4(b) and 4(c), energy trapping seems to be insensitive to H. Corresponding to $H = 0.3$, 0.4, and 0.5 mm, the resonant frequencies of the first mode are 3.826517×10^6 rad$\cdot$s^{-1}, 3.405791×10^6 rad$\cdot$s^{-1}, and 3.067456×10^6 rad$\cdot$s^{-1}, respectively. They become lower as the plate thickness increases as expected. This cannot be seen in Fig. 4(a), where the normalized frequency is used.

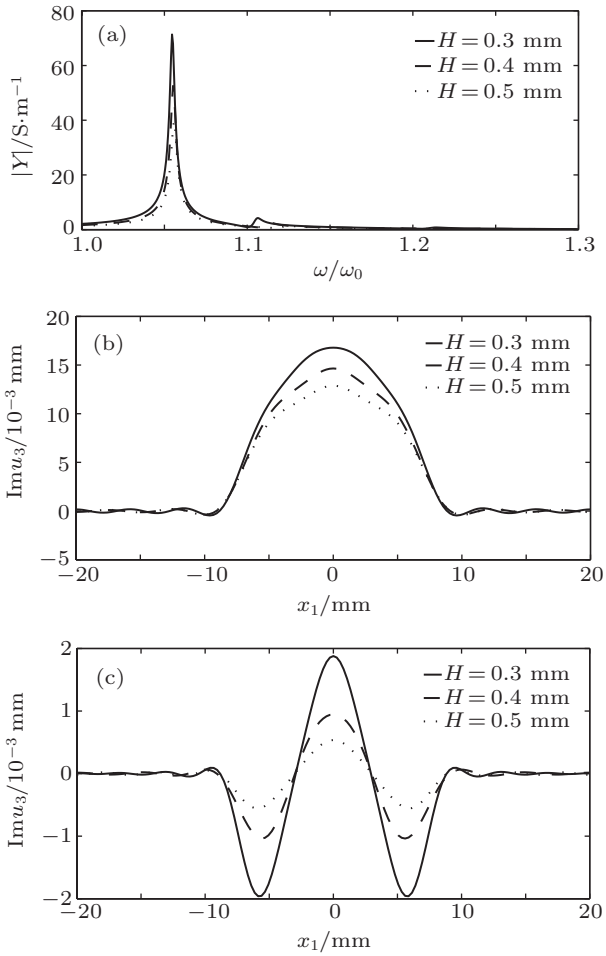


Fig. 4. The effects of H when $a = 7.5$ mm. (a) Admittance, (b) Im$\{u_3(h)\}$ of the first mode, and (c) Im$\{u_3(h)\}$ of the second mode.

5. Conclusions

An exact solution for electrically-forced vibrations of ceramic mesa resonators is obtained. The analysis is also valid for 6-mm class crystals. The admittance at the fundamental TSh resonance is much larger than that at other resonances, and is sensitive to the length and thickness of the thick central portion of the resonator. A longer and thinner central portion leads to larger admittance. Energy trapping is mainly determined by the length of the central portion and is less sensitive to its thickness. A shorter central portion has better energy trapping.

References

[1] Koga I 1932 *Phys.* **3** 70
[2] Tiersten H F 1963 *J. Acoust. Soc. Am.* **35** 53
[3] Tiersten H F 2003 *IEEE Trans. Ultrason. Ferroelect. Freq. Control* **50** 1436

[4] Mindlin R D 1965 *Int. J. Solids Struct.* **1** 141
[5] Yang Z T, Hu Y T and Yang J S 2009 *Ultrason.* **49** 401
[6] Mindlin R D and Lee P C Y 1966 *Int. J. Solids Struct.* **2** 125
[7] Yang J S and Kosinski J A 2004 *IEEE Trans. Ultrason. Ferroelect. Freq. Control* **51** 1047
[8] Tiersten H F and Smyth R C 1979 *J Acoust. Soc. Am.* **65** 1455
[9] Tiersten H F and Stevens D S 1986 *J. Acoust. Soc. Am.* **80** 1122
[10] Onoe M and Okada K 1969 *Proc. 23rd Annual Frequency Control Symp.* (Atlantic City: Institute of Electrical and Electronics Engineers)
[11] Sinha B K 2001 *IEEE Trans. Ultrason, Ferroelec. Freq. Control* **48** 1162
[12] Shen F, O'Shea S J, Lee K H, Lu P and Ng T Y 2003 *IEEE Trans. Ultrason. Ferroelect. Freq. Control* **50** 668
[13] Ishizaki A, Sekimoto H, Tajima D and Watanabe Y 1995 *Proc. IEEE Ultrasonics Symp.* (USA: Institute of Electrical and Electronics Engineers)
[14] Goka S, Sekimoto H and Watanabe Y 1999 *Proc. IEEE Int. Frequency Control Symp.* (France: Institute of Electrical and Electronics Engineers)
[15] Goka S, Sekimoto H and Watanabe Y 2000 *Proc. IEEE Int. Frequency Control Symp.* (USA: Institute of Electrical and Electronics Engineers)
[16] Sekimoto H, Goka S and Watanabe Y 2001 *IEEE Trans. Ultrason. Ferroelect. Freq. Control* **48** 1302
[17] Goka S, Tamura K, Sekimoto H, Watanabe Y and Sato T 2003 *Proc. IEEE Int. Frequency Control Symp.* (Tampa: Institute of Electrical and Electronics Engineers)
[18] Watanabe Y, Goka S, Sato T and Sekimoto H 2003 *Proc. IEEE Int. Frequency Control Symp.* (Tampa: Institute of Electrical and Electronics Engineers)
[19] Goka S, Mase Y, Sekimoto H, Watanabe Y and Sato T 2004 *Proc. IEEE Int. Frequency Control Symp.* (Montreal: Institute of Electrical and Electronics Engineers)
[20] Goka S, Mase Y, Sekimoto H and Watanabe Y 2006 *Proc. IEEE Int. Frequency Control Symp.* (Miami: Institute of Electrical and Electronics Engineers)
[21] He H J, Liu J X and Yang J S 2011 *IEEE Trans. Ultrason. Ferroelect. Freq. Control* **58** 2050
[22] Zhang H, Wang Z Q and Zhang S Y 2006 *Acta Acustica* **31** 8
[23] Mo S M, Zhao J Z, Wu G M and Chen J M 2008 *Technical Acoustics* **27** 167
[24] Du J K, Xian K, Wang J and Yang J S 2009 *Ultrasonics* **49** 149
[25] Qin L F, Chen Q M, Cheng H B and Wang Q M 2010 *IEEE Trans. Ultrason. Ferroelectr. Freq. Control* **57** 1840
[26] Cao X S, Jin F and Yang J S 2012 *IEEE Trans. Ultrason. Ferroelect. Freq. Control* **59** 2522
[27] Wang W Y, Zhang C, Zhang Z T, Liu Y and Feng G P 2009 *Chin. Phys. B* **18** 795
[28] Ma T F, Zhang C, Feng G P and Jiang X N 2010 *Chin. Phys. B* **19** 087701
[29] Ma T F, Zhang C, Jiang X N and Feng G P 2011 *Chin. Phys. B* **20** 057701
[30] Yang J S 2010 *Antiplane Motions of Piezoceramics and Acoustic Wave Devices* (Singapore: World Scientific)
[31] Bleustein J L 1969 *J. Acoust. Soc. Am.* **45** 614
[32] Tiersten H F 1969 *Linear Piezoelectric Plate Vibrations* (New York: Plenum)
[33] Auld B A 1973 *Acoustic Fields and Waves in Solids*, Vol. 1 (New York: John Willey and Sons) pp. 357–382